Electron-impact excitation of the $(3d^{10}4s)^2S_{1/2} \rightarrow (3d^9 4s^2)^2D_{5/2,3/2}$ transitions in copper atoms

O. Zatsarinny and K. Bartschat
Department of Physics and Astronomy, Drake University, Des Moines, Iowa 50311, USA

V. Suvorov and P. J. O. Teubner
School of Chemical and Physical Sciences, Flinders University, GPO Box 2100, Adelaide 5001, Australia

M. J. Brunger
ARC Centre for Antimatter-Matter Studies, School of Chemical and Physical Sciences, Flinders University, GPO Box 2100, Adelaide 5001, Australia

(Received 20 April 2010; published 9 June 2010)

Results from a joint experimental and theoretical investigation of electron impact excitation of the $(3d^{10}4s)^2S_{1/2} \rightarrow (3d^9 4s^2)^2D_{5/2,3/2}$ transitions in copper atoms are presented. The experimental results were obtained with the laser-induced fluorescence technique, while the numerical calculations were performed in a variety of nonrelativistic, semirelativistic, and fully relativistic R-matrix (close-coupling) calculations. Whereas there is qualitative agreement between the measured and predicted energy dependence of the angle-integrated cross section, significant uncertainties remain regarding the position and the height of the near-threshold maximum of the excitation function for the $(3d^9 4s^2)^2D_{3/2}$ state. These uncertainties translate into difficulties regarding the absolute normalization of the relative experimental data to the theoretical predictions.

DOI: 10.1103/PhysRevA.81.062705 PACS number(s): 34.80.Dp

I. INTRODUCTION

Electron collisions with copper atoms are of interest for both fundamental reasons and the need for accurate atomic data in modeling applications such as the copper-vapor laser (CVL), which has become a well-established source of high-power visible light [1]. From a fundamental point of view, copper is a very difficult target to describe theoretically, due to the alkali-metal-like characteristics of its $3d^{10}nl$ single-electron valence states that are mixed with the $3d^9nln'l'$ two-electron helium-like states on the open $3d^9$ doubly ionized core. This mixture leads to a strong term dependence of the $3d$ core and all valence orbitals, and it is likely to become a serious problem in close-coupling calculations when both of these sets of target states are included in the expansion of the total scattering wave function.

As summarized in a recent paper on electron impact excitation of the $(3d^{10}4s)^2S \rightarrow (3d^{10}4p)^2P$ resonance transition [2], a significant amount of effort, both experimentally and theoretically, has been devoted over the past several decades to the understanding of this particular collision process, due to its importance in the understanding of the CVL laser. Although excitation from the ground state is weak, detailed knowledge about the $(3d^{10}4s)^2S \rightarrow (3d^9 4s^2)^2D$ forbidden transition is equally important, since the ^2D state is part of a three-level system for pulsed-laser operation. Consequently, the cross sections for these excitation processes are amongst the most important parameters needed in modeling the CVL [3].

Unlike the extensive work on the resonance transition (see [2] for a list of references), studies of the weak $(3d^{10}4s)^2S \rightarrow (3d^9 4s^2)^2D$ excitation process have been scarce. In fact, we are not aware of additional work beyond the four-state R-matrix (close-coupling) calculation by Scheibner *et al.* [4] and an unpublished followup 10-state study by Scheibner and Hazi [5] that effectively confirmed their earlier work.

The lack of existing studies for the above transition is most likely related to the difficulties faced by both experimentalists and theorists alike. Experimentally, the signal is weak and there is no radiation emitted after excitation of the ^2D state, while theoretically the term dependence of the $3d$ and $4s$ orbitals, as well as the need to include coupling to higher excited states for such a weak transition, presents a major challenge.

A way to address these challenges for the closely related problem in electron collisions with gold atoms was outlined in our two joint recent studies for electron impact excitation of the $(5d^{10}6s)^2S_{1/2} \rightarrow (5d^{10}6p)^2P_{1/2,3/2}$ resonance transitions [6] and the $(5d^{10}6s)^2S_{1/2} \rightarrow (5d^9 6s^2)^2D_{5/2,3/2}$ optically forbidden transitions [7]. Similar to copper, knowledge of these cross sections, as well as accurate energy levels and oscillator strengths, are important to understand the details of the gold-vapor laser (GVL). Experimentally, the excitation of the $(5d^9 6s^2)^2D_{3/2}$ state could be studied by further excitation of this state to the $(5d^{10}6p)^2P_{1/2}$ state by a laser and then observing the laser-induced fluorescence (LIF) signal from the $(5d^{10}6p)^2P_{1/2} \rightarrow (5d^{10}6s)^2S_{1/2}$ transition back to the ground state. The very same technique was used in the present work for the copper target.

Theoretically, a highly promising method to account for the term dependence of the one-electron orbitals in the various target states of interest is the B-spline R-matrix method developed by Zatsarinny and coworkers over the past decade [8–10]. A nonrelativistic version of the computer code, which can also treat relativistic effects as a perturbation at the level of the Breit-Pauli approximation, was published by Zatsarinny [11]. The above-mentioned calculations for e-Au collisions [6,7], on the other hand, were actually performed with a fully relativistic extension of the package. While the agreement with experiment obtained with this approach, which treats the most important physical effects (Coulomb interaction, electron exchange, channel coupling, core-valence, and inner-core correlations) in a fully ab initio manner, was quite satisfactory, a few discrepancies remained. In particular, it proved to be very difficult to reproduce the experimental position of a strong

maximum seen in the excitation function of the $(5d^9 6s^2)^2 D_{3/2}$ state.

In order to better understand the intricacies of these collision processes and hopefully to obtain additional clues about possible reasons for the remaining differences between experiment and theory, studying copper with an atomic number of $Z = 29$ instead of gold ($Z = 79$) as a target is very promising from a theoretical point of view, since one can expect even a nonrelativistic model to be at least somewhat appropriate after simply recoupling the results to account for the different states of total electronic angular momentum J. At the same time, some improvement, without drastic changes in the qualitative appearance of the results, seems likely when relativistic effects are accounted for at the Breit-Pauli or ultimately at the Dirac-Coulomb level. The promise of simultaneously being able to provide data of interest for the modeling community, therefore, provided the motivation for the present work, which complements our recent study of the resonance transition [2].

In the next section we describe our apparatus and measurement technique. This is followed by a description of various nonrelativistic, semirelativistic, and fully relativistic close-coupling calculations that were performed for this work. After presenting and discussing our results, we finish with some conclusions from the present study.

II. EXPERIMENTAL DETAILS

In this study we used the Type I stepwise excitation technique of MacGillivray and Standage [12], in conjunction with the Lamb-dip technique [13], in order to measure the excitation cross sections for the $4\,^2S_{1/2} \rightarrow 3\,^2D_{3/2}$ transition in copper. The incident electron energies were in the range from 1.6 eV (threshold) to 4.8 eV for this work. The major complication in these experiments, over those we previously reported for electron impact excitation of the $4\,^2P$ state [2], was the contamination of the incident copper beam with metastable states that were thermally excited according to the Gibbs distribution. The solution to this problem, which was described in detail by Suvorov [14], involved the introduction of a counterpropagating laser to facilitate the use of the Lamb dip.

A schematic diagram of the experimental geometry used in the stepwise excitation measurements of the ^2D state cross sections is given in Fig. 1. As a description of the main components of the apparatus, namely the vacuum chamber, the electron gun with the electron beam chopper and Faraday cups, the copper oven, and the photon detection system, were given before [2], we do not repeat them here unless required for this specific experiment.

The copper atoms were produced by heating copper wire in a molybdenum oven that was heated by electron bombardment to ~1550 K. These copper atoms, traveling with a mean speed of 800 m/s in a beam of 6.5-mm diameter, passed through a laser beam that had a Gaussian profile and was 2.3 mm in diameter (see Fig. 1). The frequency of the laser (Spectra-Physics 380 D ring dye laser pumped with a Coherent INNOVA 320 argon ion laser) was typically locked by an electronic servo-system to the $^2D_{3/2} \rightarrow {}^2P_{1/2}$ ($F = 0 \rightarrow 1$) hyperfine

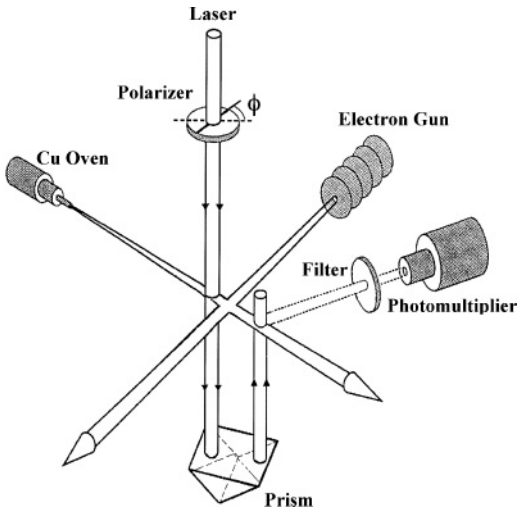

FIG. 1. Experimental configuration for the laser-induced fluorescence technique measurements.

(HFS) transition, hereafter referred to as "peak 6" [14]. This latter designation arises as, when the 578.2-nm probe laser has its frequency varied over 13 GHz, six possible $^2D_{3/2} \rightarrow {}^2P_{1/2}$ HFS transitions can be excited. The copper beam, which has now had the thermally excited D states quenched to the ground state to some degree, was then intersected by an electron beam of 5-mm diameter and known energy (see below). It is these electrons that excite the ground state ($4\,^2S_{1/2}$) copper atoms to the $3\,^2D_{3/2}$ state. A corner cube (see Fig. 1) was used to reflect the incident laser beam back through the atomic beam, but displaced by 16 mm along the atomic beam axis from the original point of entry. The atoms then entered the field of the reflected laser beam, and those in the metastable $3\,^2D_{3/2}$ state underwent a transition to the $4\,^2P_{1/2}$ state and subsequently decayed to the ground state. Radiation of 327.4 nm [2] arising from this interaction region was collected by a fused silica lens, passed through an interference filter, and was finally detected on a low-noise photomultiplier tube (PMT). The solid angle of the photon detector was determined by the silica lens and had a value of 0.66 steradians.

The interference filter we employed had a bandpass of 10 nm centered at 330 nm, with a transmittance of ~12% at 325 nm and ~32% at 327 nm. Our THORN EMI 98999B PMT was configured so that observations were made at the "magic" angle of 54.7° with respect to the laser beam. Thus, the influence of anisotropy in the measured impact fluorescence was minimized. Pulses from the PMT were amplified by a preamplifier and a delay line amplifier. They were then passed through a discriminator before being fed into a pair of gated counters, whose gates were generated by a reference signal derived from the rotating toothed wheel that modulated ("chopped") the reflected laser beam. Thus, one counter was enabled when the reflected laser beam was in the scattering chamber (i.e., it counted the scattered signal from the beam plus background, N_a), while the other counted the scattered signal when the reflected laser beam was off (i.e., the background signal N_b). After every 0.5 s, which was the electron chopper preset time in this work, the count rate was

given by

$$N^{0.5} = N_a^{0.5} - N_b^{0.5}. \quad (1)$$

In addition, these pulses were counted separately during the time intervals when the electron beam was either present (on) at the interaction region or chopped off. This procedure was necessary in order to discriminate between signal from background metastable states (as our Lamb-dip approach was not 100% efficient in quenching the thermal population in these levels) and those excited by the electron beam. In practice, this was achieved by modulating (chopping) the voltage on the anode of the electron gun [2,14]. In this way, the number of true counts scattered from the copper beam, which is proportional to the $3\,^2D_{3/2}$ integral cross section of interest, could be determined at each energy from

$$N^{300} = \sum_{300} N_{\text{on}}^{0.5} - \sum_{300} N_{\text{off}}^{0.5}. \quad (2)$$

This gives the true signal counted for a nominal present time of 300 s. This photon count rate was then adjusted to unit electron beam current for each energy, and thus the relative excitation function was determined.

The preset count rate in these experiments was determined by the frequency stability of the laser. Despite our use of the Fabry-Perot etalons of the Spectra-Physics 385 external reference interferometer and our Lamb-dip technique, laser stability for periods of 300–600 s was only possible with the limit on the counting time being due to "mode hops" induced by temperature fluctuations in both the laser dye and laser optics. Nonetheless, such a stability window was sufficient for these measurements. The typical electron-induced photon signal was 5–10 Hz at 2 eV and up to 40 Hz at 2.5–3 eV. Although this signal was of reasonable intensity, it was the signal-to-noise (S/N) ratio that presented a major challenge to the present experiments. The reason for the S-N ratio to be lower at the higher energies of this investigation is the excitation threshold of the $4\,^2P$ state at 3.8 eV. Photons arising from direct electron excitation of the 4^2P state, therefore, increasingly contributed to the background as the energy was increased beyond 3.8 eV. Indeed, this problem restricted the present investigations to a maximum electron energy of 4.8 eV. At the lower energies the S-N ratio was also found to be low, with the noise now being caused by the initial thermal population of the $3\,^2D_{3/2}$ state due to the temperature of the oven. Note that in all our measurements, at each energy, we established that the fluorescent photon signal was linear with the electron beam current.

It should now be apparent that we measured the relative excitation cross section for the HFS $3\,^2D_{3/2}$ level with quantum number $F = 0$. The question, however, remains as to how accurately this excitation function reflects that for the $3\,^2D_{3/2}$ state as a whole. This issue is addressed by the Percival-Seaton hypothesis [15], which states that the nuclear spin plays no effective role in electron-atom collisions: in other words, the HFS can be ignored in the collision. To test this hypothesis explicitly in the present experiment, we repeated our measurements, this time with the laser tuned to excite the $^2D_{3/2} \rightarrow {}^2P_{1/2}(F = 3 \rightarrow 2)$ HFS transition. This measurement, labeled "peak 1," is shown together with the earlier measurement "peak 6" in Fig. 2. In order to compare

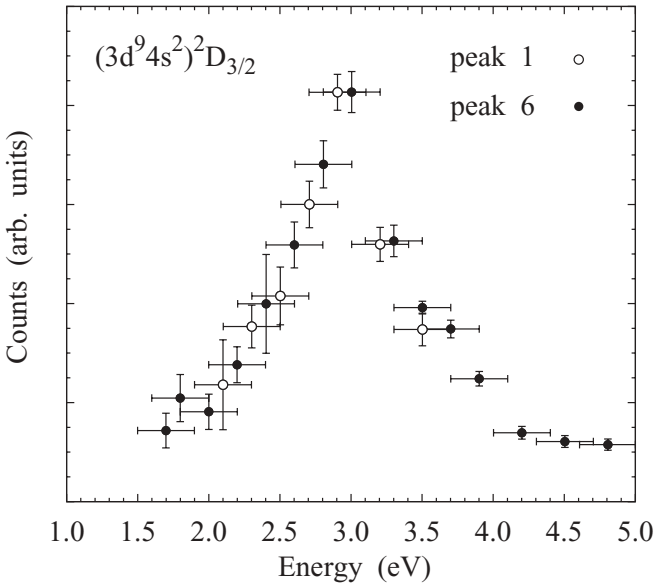

FIG. 2. Measured excitation function of the $(3d^94s^2)^2D_{3/2}$ state in copper using two different HFS transitions. In order to compare the two relative measurements, they were normalized to each other at the peak. See text for more details. No scale is given on the y axis, since the measurements are not absolute.

these two relative measurements, they were normalized to each other at the peak. It is clear from Fig. 2 that both sets of data are in good accord with one another. We therefore conclude that the Percival-Seaton hypothesis holds for our experiment, and thus our $3\,^2D_{3/2}$ cross section determined from the HFS $F = 0$ level is indeed representative of that for the $3\,^2D_{3/2}$ manifold.

The final difficulty in the present measurements revolves around our choice of an indirectly heated oxide cathode as the electron source. While the energy resolution of this cathode [$\Delta E \sim 0.3$ eV, full width at half maximum (FWHM)] is superior to that which can be achieved with a W-hairpin filament, it is well known from $(e,2e)$ studies [16] that under extreme conditions (such as we had here) the emission properties of those oxide cathodes can vary significantly over time. In particular, this manifests itself as a change in the true value of the incident beam energy over time. In the case of the $(e,2e)$ work [16], where data were collected over a period of several weeks to a month, the shift in the true value of the beam energy could be as much as ± 500 meV. Our measuring times, however, are much shorter than this, and thus we conservatively estimate the uncertainty in our beam energy calibration to be about ± 200 meV. Certainly our energy calibration, against the b feature in the metastable excitation function of neon [17], both before and after a measurement, suggests that such a value is reasonable. It is reflected by the x-error bars on our experimental cross-section plots.

Finally, we note that all the data collection and analysis were performed under computer control, with full details being found in Ref. [14].

III. COMPUTATIONAL METHOD

The numerical calculations for the present work were based on several approaches that will be described in some

detail in the subsections below. They consist of nonrelativistic and semirelativistic R-matrix (close-coupling) expansions using the standard code RMATRIX-I of the Belfast group [18] (Sec. III A) or the B-spline R-matrix code BSR of Zatsarinny [11], including a fully relativistic Dirac-Coulomb treatment using the recently developed DBSR code [7,10] (Sec. III B). We believe that the latter calculation should provide the best theoretical description, and hence it will be described in the most detail. We will also present results generated by Scheibner *et al.* [4] and later by Scheibner and Hazi [5] who used a nonrelativistic version of the Belfast code as well.

A. Standard R-matrix calculations

In order to get a first impression about the results to be expected, we performed a straightforward nonrelativistic R-matrix calculation with the RMATRIX-I code [18]. In this model, we closely coupled the ground state $(3d^{10}4s)^2S$ and the excited states $(3d^9 4s^2)^2D$, $(3d^{10}4p)^2P$, and $(3d^{10}4d)^2D$, respectively, thus forming a four-state model that will be referred to as RM4 below. For the structure description we started with the one-electron orbitals $1s$, $2s$, $3s$, $4s$, $2p$, $3p$, and $3d$ for the $(3d^{10}4s)^2S$ ground state as given by Clementi and Roetti [19]. We then employed the structure program CIV3 of Hibbert [20] to reoptimize the $3d$ and $4s$ orbitals in order to get a reasonable, though certainly not perfect, description of both the $(3d^{10}4s)^2S$ and the $(3d^9 4s^2)^2D$ states. We then generated a correlated $\bar{5}d$ pseudoorbital in order to increase the flexibility by being able to build suitable linear combinations of the $4d$ and $\bar{5}d$ orbitals for each target state of interest. Finally, we used all configurations that could be built with one electron above the $3d^{10}$ singly ionized core or with two electrons above the $3d^9$ doubly ionized core by occupying one or two of the $4p$, $4d$, and $\bar{5}d$ orbitals that were also generated with CIV3 [20]. Using this method accounts to a significant extent for the term dependence in the one-electron orbitals and made it possible to obtain the excitation energies of the $(3d^9 4s^2)^2D$ and $(3d^{10}4p)^2P$ states from the ground state to an accuracy of better than 0.1 eV.

In order to allow for a direct comparison with experiment, the diagonal elements of the Hamiltonian matrices for each $(N+1)$-electron symmetry were then adjusted to produce the correct experimental thresholds. While this is a standard procedure in the Belfast code, any adjustment of the N-electron target energies carries the danger of producing an inconsistency between the N-electron target and the $(N+1)$-electron collision treatments, since there is no unique way of simultaneously adjusting the $(N+1)$-electron bound-bound terms in the expansion of the R-matrix basis functions. The need for these latter terms arises from the numerical requirement of the code to use a single set of mutually orthogonal one-electron orbitals to describe both the bound and the scattering states. We also checked that pseudoresonances do not present a problem for this model in the low-energy regime of interest for the present work.

This four-state model is expected to produce similar results to those obtained by Scheibner *et al.* [4] (denoted as RM4-SHH) below, with potential differences being due to a different way of optimizing the target orbitals and/or the adjustment procedure for the excitation thresholds. While Scheibner and Hazi [5] further extended this work by performing a 10-state calculation (RM10-SH), details of this extension are, unfortunately, not available to us.

As an extension of the above RM4 model, we then performed a semirelativistic calculation, in which we included the one-electron spin-orbit term as a first-order perturbation in calculating the relevant matrix elements. This "Breit-Pauli" model will be referred to as RM7-BP below. We used an R-matrix radius of $a = 25.8a_0$, with $a_0 = 0.529 \times 10^{-10}$ m being the Bohr radius, and employed 15 basis functions for each orbital angular momentum l to expand the continuum wave function of the projectile electron inside the R-matrix box. The scattering calculations were performed for partial waves up to total orbital angular momenta of $L = 8$ or total electronic angular momenta $J = 8$, respectively. This was sufficient to obtain partial-wave converged results in the near-threshold regime for the optically forbidden transitions of interest for the current paper.

B. B-spline R-matrix calculations

As mentioned previously, an important aspect for a relatively complex target such as copper is the structure description, which is by no means trivial. A particular difficulty in copper is the filled and very diffuse $3d$ subshell. Recall that part of the Cu spectrum consists of Rydberg-like $(\ldots 3d^{10}nl)$ states, while the two lowest excited states, which are the topic of this paper, have the dominant configuration $3d^9 4s^2$. Hence, one can expect a significant configuration dependence of the $3d$ and $4s$ orbitals, as well as coupling between single-electron valence and core-excited states.

The distinguishing features of the BSR method [11] are (i) the ability to use term-dependent, and, hence, nonorthogonal sets of one-electron orbitals in the target description, and (ii) B splines as the underlying, effectively complete basis to expand the wave function of the projectile. Furthermore, it is an all-electron approach, and, hence, core-valence correlation effects (such as the core polarization) can be described ab initio.

For the first set of states for neutral copper with dominant configurations $3d^{10}nl$, the principal correlation effects originate from the interaction of the valence electron with the core, whereas for the core-excited $3d^9 4s^2$ and $3d^9 4s 4p$ states the valence correlation itself is also important. In the present approach, we included the core-valence correlation ab initio by adding target configurations with an excited core. However, direct multiconfiguration calculations in this case usually lead to very large expansions, which can hardly be used in subsequent scattering calculations. For this reason, we used the bound-state close-coupling method to generate the target states. This method also provides a way to accurately describe the strong interaction between the valence and core-excited states.

Specifically, the calculation of the target states included the following steps. We started by generating the core orbitals from a Cu^{2+} Hartree-Fock calculation for the $3d^9$ core. Next, the excited $4s$ and $4p$ orbitals were generated in a frozen-core calculation for $Cu^+ 3d^9 nl$, and the entire spectrum of Cu was

represented by the expansion,

$$\Phi(LS\pi) = \mathcal{A}\sum_i \{\varphi(3d^{10})\phi(n_i l_i)\}^{LS\pi} + \mathcal{A}\sum_i \{\varphi(3d^9 4s)\phi(n_i l_i)\}^{LS\pi} + \mathcal{A}\sum_i \{\varphi(3d^9 4p)\phi(n_i l_i)\}^{LS\pi} + a\varphi(3d^9 4s^2), \tag{3}$$

where $\mathcal{A}$ denotes the antisymmetrization operator. Here, the first term represents the valence $3d^{10}nl$ states, while the second term represents the core-excited $3d^9 4snl$ states. The third term is included primarily to introduce the core-valence correlation for the valence states due to the strong $3d \rightarrow 4p$ excitation. This term also describes the valence correlation for the core-excited states due to $4s \rightarrow 4p$ excitation. For example, it accounts for the strong configuration mixing between the $3d^9 4s4p$ and $3d^9 4p4d$ states.

We found, however, that the accuracy of the relative position of the levels crucially depends on the choice of the $3d^{10}$ core wave function in this expansion. For example, choosing the $3d^{10}$ wave function from fully relaxed Hartree-Fock calculations for $Cu^+(3d^{10})$ results in large errors in the relative position of the valence and core-excited states, as well as in a very poor description of the core-valence correlation for the $3d^{10}nl$ states. This is due to the large radial correlation in the $3d^{10}$ core. Therefore, employing the same one-electron radial function for all $3d$ electrons is entirely inappropriate for this case. A solution to the problem was found by Froese Fischer [24]. She suggested using a partially extended Hartree-Fock model for the description of the $3d^{10}$ core wave function, in which the last $3d$ orbital is not constrained to be the same as the other nine. Specifically, the core wave function is represented as a combination of the $3d^{10}$ and $3d^9\bar{4}d$ configurations, where the $3d$ orbital is the one from the $Cu^{2+}(3d^9)$ state while the correlated $\bar{4}d$ orbital is optimized on the $Cu^+(3d^{10})$ ground state. The mixing coefficients between the $3d^{10}$ and $3d^9\bar{4}d$ configurations were found to be 0.93 and 0.36, respectively, thus indicating a strong interaction. Note that the mean radius of the $\bar{4}d$ orbital is $2.2a_0$, whereas the mean radius of the $3d$ orbital is only $0.9a_0$. This reflects the extensive radial correlation in the very diffuse $3d$ subshell.

The core-excited $(3d^9 4s^2)^2D$ state cannot be described accurately with the expansion (3). It was therefore considered in separate multiconfiguration Hartree-Fock (MCHF) calculations. The expansion contained all configurations with promotion of two valence electrons to the set of $\{\bar{5}s,\bar{5}p,\bar{5}d,\bar{5}f\}$ correlated orbitals. Note that we employed fully relaxed $3d,4s$ and $\bar{5}l$ correlated orbitals in this case. These orbitals, therefore, are not orthogonal to the orbitals in the $3d^{10}nl$ states. The relaxation effects were found to be very important in the present case, leading to corrections in the excitation energies of up to 0.5 eV. All the above calculations were carried out in the Hartree-Fock approximation using the MCHF atomic structure package [21]. In order to obtain a consistent description with all the other states of the $^2D^e$ term, the multiconfiguration expansion of the $(3d^9 4s^2)^2D$ state was then incorporated into the expansion (3).

The final Cu target wave functions were generated with the B-spline box-based close-coupling approach [22]. The unknown radial components for the outer valence electron $\phi(n_i l_i)$ in expansion (3) were expanded in a B-spline basis. The coefficients of the B-spline expansions were found by diagonalizing either the nonrelativistic or the Breit-Pauli Hamiltonian (the latter only including all one-electron relativistic terms), with the additional requirement that the wave functions vanish at the boundary. Note that we do not impose orthogonality of the valence orbitals nl to the correlated orbitals $\bar{n}l$ in the above procedure. This speeds up the convergence of expansion (3) and yields accurate binding energies with a relatively small number ($\sim$50) of correlated configurations for each symmetry. More details of this procedure can be found in [8].

The number of physical states that we can generate in this method depends upon the size a of the R-matrix box. Choosing $a = 60\ a_0$ allowed us to obtain a good description for all low-lying Rydberg-type bound states of Cu up to $n = 7$. The resulting spectra also contain the core-excited states with configurations $(3d^9 4s^2)$ and $(3d^9 4s4p)$, respectively. Similar to what we will show for the fully relativistic model in Table I below, the resulting target excitation energies agreed with the experimental values to much better than 0.1 eV.

We first performed a 20-state nonrelativistic collision calculation (to be referred to as BSR20 below) and then the corresponding 34-state semirelativistic (BSR34-BP) calculation, closely coupling all the states with principal configurations $(3d^{10}4s)$, $(3d^{10}4p)$, $(3d^{10}4d)$, $(3d^{10}5s)$, $(3d^{10}5p)$, $(3d^{10}6s)$, $(3d^9 4s^2)$, and $(3d^9 4s4p)$. Partial-wave contributions up to a total electronic angular momentum of 25 for the collision system were calculated numerically to ensure partial-wave converged results for the transitions and energies under consideration. The cross sections were calculated in the same way as in the standard R-matrix approach by employing the package FARM of Burke and Noble [25] to solve the collision problem outside of the R-matrix box for each collision energy of interest and match to the inner-region solution at the boundary.

The final set of numerical calculations performed for this work was based upon the fully relativistic Dirac B-spline R-matrix (DBSR) method [10], which was also used in similar calculations for e-Au [6,7] collisions. The general philosophy in generating the target description was the same as described above for the nonrelativistic and semirelativistic BSR models, except that we now used Dirac spinors and performed the calculation in the multiconfiguration Dirac-Fock approximation by employing the GRASP2K relativistic atomic structure package [23].

The spectrum of Cu was again recalculated using a B-spline box-based expansion similar to (3), except that the unknown large and small radial components for the outer valence electron, $\phi(n\ell)$, were expanded in separate B-spline bases as

$$P(r) = \sum_{i=1}^{n_p} p_i B_i^{k_p}(r), \tag{4}$$

$$Q(r) = \sum_{i=1}^{n_q} q_i B_i^{k_q}(r). \tag{5}$$

TABLE I. Calculated and observed [26] excitation energies for the Cu states included in the 34-state (DBSR34) close-coupling expansion. Also given are the absolute energies (in atomic units) obtained in the structure calculation. $4s4p$ and $4s4p'$ stands for the $(4s4p)^3P$ and $(4s4p')^1P$ coupling, respectively.

State	Theory (a.u.)	Theory (eV)	Experiment (eV)	Difference (eV)
$(3d^{10}4s)^2S_{1/2}$	−1653.566005	0.000	0.000	0.000
$(3d^94s^2)^2D_{5/2}$	−1653.514944	1.389	1.389	0.000
$(3d^94s^2)^2D_{3/2}$	−1653.505775	1.639	1.642	−0.003
$(3d^{10}4p)^2P_{1/2}$	−1653.426999	3.782	3.786	−0.003
$(3d^{10}4p)^2P_{3/2}$	−1653.425550	3.822	3.817	0.005
$(3d^94s4p)^4P_{5/2}$	−1653.389392	4.806	4.838	−0.032
$(3d^94s4p)^4P_{3/2}$	−1653.384817	4.930	4.974	−0.043
$(3d^94s4p)^4F_{9/2}$	−1653.380967	5.035	5.072	−0.037
$(3d^94s4p)^4P_{1/2}$	−1653.380320	5.053	5.076	−0.024
$(3d^94s4p)^4F_{7/2}$	−1653.378977	5.089	5.102	−0.013
$(3d^94s4p)^4F_{5/2}$	−1653.376827	5.148	5.153	−0.006
$(3d^94s4p)^4F_{3/2}$	−1653.373811	5.230	5.245	−0.015
$(3d^{10}5s)^2S_{1/2}$	−1653.368220	5.382	5.348	0.033
$(3d^94s4p)^4D_{7/2}$	−1653.367368	5.405	5.395	0.010
$(3d^94s4p)^2F_{5/2}$	−1653.366395	5.431	5.421	0.010
$(3d^94s4p)^4D_{5/2}$	−1653.363459	5.511	5.506	0.006
$(3d^94s4p)^4D_{3/2}$	−1653.362855	5.528	5.523	0.005
$(3d^94s4p)^4D_{1/2}$	−1653.362743	5.531	5.569	−0.038
$(3d^94s4p)^2F_{7/2}$	−1653.361385	5.568	5.575	−0.007
$(3d^94s4p)^2P_{1/2}$	−1653.359587	5.617	5.681	−0.064
$(3d^94s4p)^2P_{3/2}$	−1653.358482	5.647	5.688	−0.042
$(3d^94s4p)^2D_{3/2}$	−1653.355733	5.722	5.725	−0.003
$(3d^94s4p)^2D_{5/2}$	−1653.353591	5.780	5.777	0.002
$(3d^{10}5p)^2P_{3/2}$	−1653.340943	6.124	6.123	0.001
$(3d^{10}5p)^2P_{1/2}$	−1653.340752	6.129	6.123	0.007
$(3d^{10}4d)^2D_{3/2}$	−1653.338209	6.198	6.191	0.007
$(3d^{10}4d)^2D_{5/2}$	−1653.338189	6.199	6.192	0.007
$(3d^{10}6s)^2S_{1/2}$	−1653.324905	6.560	6.552	0.008
$(3d^94s4p')^2F_{7/2}$	−1653.311688	6.920	6.947	−0.027
$(3d^94s4p')^2P_{3/2}$	−1653.309644	6.976	6.986	−0.010
$(3d^94s4p')^2D_{5/2}$	−1653.308245	7.014	7.024	−0.010
$(3d^94s4p')^2F_{5/2}$	−1653.302722	7.164	7.206	−0.042
$(3d^94s4p')^2P_{1/2}$	−1653.300226	7.232	7.236	−0.004
$(3d^94s4p')^2D_{3/2}$	−1653.299521	7.251	7.277	−0.026

As before, the coefficients of the B-spline expansions, plus the sets of p_i and q_i, were found by diagonalizing the Dirac-Coulomb Hamiltonian.

Tables I and II illustrate the accuracy of the target description that was obtained in the present DBSR calculation for both the energy levels of the states included and the oscillator strengths for transitions between the lowest five states of Cu. Our values are in excellent agreement with the experimental data [26] and with the few oscillator strengths given in the last NIST compilation by Sansonetti and Martin [27]. This good agreement with experiment for the structure part of the problem gives us confidence in the accuracy of our approach.

The total wave function for each partial-wave symmetry of the collision problem was also constructed from four-component Dirac spinors. Note that the radial functions for the large and small components were expanded in separate B-spline bases of different order (8 and 9, respectively). This allowed us to avoid the occurrence of spurious pseudostates [28]. We used a semiexponential grid for the B-spline knot sequence and a relatively large number (159) of splines to cover the inner region up to the R-matrix radius of $60a_0$. This large number of splines was required to correctly describe the finite-size nuclear model, with a Fermi potential adopted in the present work. Partial-wave contributions up to a total angular momentum $J = 25$ were included in the calculations. With up to 158 different scattering channels in the present DBSR34 model, Hamiltonian matrices of rank as large as 50 000 were set up in the B-spline basis and had to be diagonalized in the internal region. In order to perform the present calculations, we parallelized our BSR codes with MPI and employed the SCALAPACK libraries [29].

TABLE II. Comparison of calculated and observed oscillator strengths for selected transitions in Cu.

Transition	This work	Experiment [27]
$(3d^{10}4s)^2S_{1/2} \rightarrow (3d^{10}4p)^2P_{1/2}$	0.207	0.219
$(3d^{10}4s)^2S_{1/2} \rightarrow (3d^{10}4p)^2P_{3/2}$	0.419	0.433
$(3d^94s^2)^2D_{5/2} \rightarrow (3d^{10}4p)^2P_{3/2}$	0.0057	0.0052
$(3d^94s^2)^2D_{3/2} \rightarrow (3d^{10}4p)^2P_{1/2}$	0.0038	
$(3d^94s^2)^2D_{3/2} \rightarrow (3d^{10}4p)^2P_{3/2}$	0.0009	

IV. RESULTS AND DISCUSSION

Figures 3 and 4 exhibit a comparison of our predictions from the various calculations described above with the present experimental data in the near-threshold regime. Recall that the measurements are confined to impact energies less than about 5 eV. Furthermore, the experimental numbers are relative (i.e., they can be scaled by any positive number). Hence,

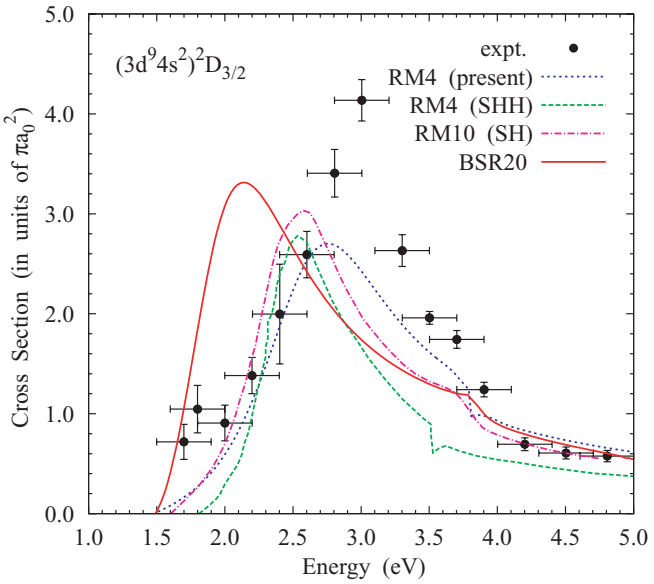

FIG. 3. (Color online) Excitation function of the $(3d^94s^2)^2D_{3/2}$ state in copper. The results from various nonrelativistic R-matrix calculations are compared with the present experimental data. The relative experimental data were visually normalized to the theories shown in Fig. 4 below. See text for details.

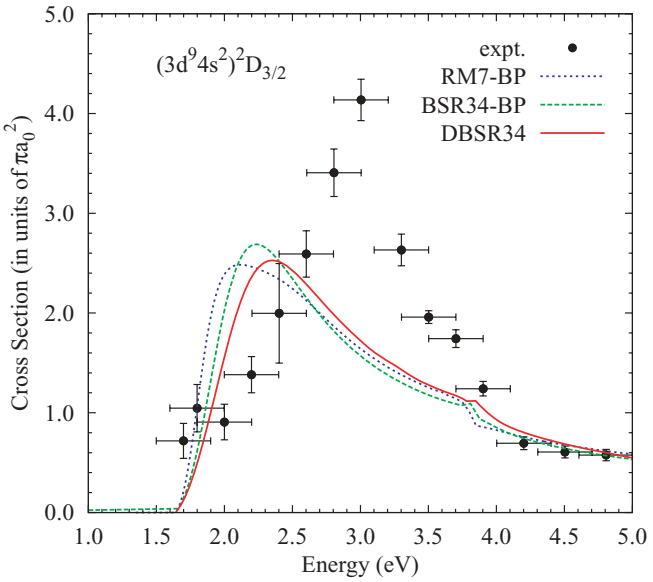

FIG. 4. (Color online) Excitation function of the $(3d^94s^2)^2D_{3/2}$ state in copper. The results from various semirelativistic and fully relativistic R-matrix calculations (see text for details) are compared with the present experimental data. The latter were visually normalized to the theories above 4 eV. See text for details.

the normalization chosen in these figures reflects one of several possibilities. In this case, there is relatively good agreement between experiment and essentially all theories at the three highest energy points for which the measurement was performed. Had one normalized to the height of individual theoretical peaks, the experimental data would be multiplied by factors as small as about 0.6. Hence, we estimate the confidence of the absolute values to be within a factor of 0.5–1.1 relative to the numbers displayed in the graph.

Similarly to our recent work on the electron impact excitation function of the $(5d^96s^2)^2D_{3/2}$ level in gold [7], it is apparently very difficult to reproduce the measured shape of the excitation function, in particular the cross-section maximum. In the present case of the copper target, all theoretical models predict the peak of the cross section at a lower energy than the measurements that show the largest value at an incident energy of ~3 eV.

Interestingly, Fig. 3 indicates that the best agreement with experiment is obtained in the nonrelativistic RM4 model. As expected, the four-state model of Scheibner *et al.* [4] produces very similar results, as does the unpublished 10-state calculation of Scheibner and Hazi [5]. Although we do not know all the details about these calculations, it is very likely that the small differences between the results from these three standard R-matrix calculations are mostly due to small differences in the structure description, including the adjustment procedure for the target thresholds, and a relatively small influence of additional channel coupling in the 10-state model. Most disturbing from a theoretical point of view, however, is the fact that the presumably best nonrelativistic model, namely the 20-state BSR calculation, predicts the cross-section maximum at an even lower energy than the other models, thereby increasing the discrepancy between theory and experiment. This discrepancy could be reduced slightly by shifting the threshold of the nonrelativistic ^2D state to the proper position of the $^2D_{3/2}$ state, in addition to just multiplying the nonrelativistic results by the statistical factor of 0.4. However, the shift is only about 0.15 eV.

Moving on to Fig. 4, we see that the discrepancies are not resolved by presumably improving the theoretical models through accounting for relativistic effects, either at the Breit-Pauli or even at the fully relativistic model. Starting with the RM7-BP model, which is based on our nonrelativistic RM4 ansatz, we see a significant move of the cross-section maximum, again to lower energies. The strong sensitivity of these results to the inclusion of just the spin-orbit interaction is somewhat surprising and shows the potential danger of calculating matrix elements of operators using wave functions that were constructed without accounting for these effects in the first place.

Compared to the corresponding nonrelativistic BSR20 model, the 34-state semirelativistic BSR ansatz yields essentially no change in the predicted position of the cross-section maximum just above 2.2 eV. The magnitude, however, drops by about 20% compared to the nonrelativistic value. This indicates that relativistic effects for this problem may indeed be important and should be treated as accurately as possible. The latter is done in the corresponding fully relativistic DBSR34 model, whose results are indeed noticeably different from those obtained with the BSR34-BP approach. These differences are a combination of the differences in the description of both the target structure and the collision problems. However, as one would expect from a relatively light target such as copper, the changes are at the level of a few percent, with the largest modifications occurring near the cross-section maximum. With this maximum being slightly further away from threshold in the DBSR34 calculation compared to that obtained in the BSR34-BP model, the lower height and a slightly broader width would be expected.

Finally, we note that all theoretical models, except for the RM4 model of Scheibner and Hazi [4] that most likely still suffers from problems with the theoretical thresholds, predict nearly the same value of $\approx 0.6\pi a_0^2$ at incident energies between 4.2 and 4.8 eV, in good agreement with the experimentally determined energy dependence. Such good agreement away from the resonance region would be expected for the present case and provides some assurance regarding the overall correctness of the numerical models.

While it may be significantly more difficult to calculate the resonance features than the background cross section, only a severe omission of an important target-structure or channel-coupling effect would be able to explain the remaining differences between experiment and the DBSR34 theory regarding the position of the cross-section maximum. Unfortunately, none of the calculations performed in the current work provides a clear indication of how to significantly improve the theory in order to obtain better agreement with experiment.

Clearly, the remaining discrepancies between theory and experiment mentioned above make it very difficult to assign reliable absolute values to the experimental data points. On the other hand, it is these absolute numbers that are needed in modeling applications. Given that the experimental peak

TABLE III. Absolute experimental values for the electron impact excitation cross section of the $(3d^{10}4s)^2S_{1/2} \rightarrow (3d^9 4s^2)^2 D_{3/2}$ transition in copper. The uncertainties given are due to statistics and reproducibility. We estimate the absolute scale to be reliable within a factor of 0.5–1.1. See text for details.

Energy (eV)	Cross section (πa_0^2)
1.7	0.72 ± 0.17
1.8	1.05 ± 0.24
2.0	0.91 ± 0.18
2.2	1.38 ± 0.18
2.4	2.0 ± 0.5
2.6	2.6 ± 0.23
2.8	3.41 ± 0.24
3.0	4.14 ± 0.21
3.3	2.64 ± 0.16
3.5	1.97 ± 0.07
3.7	1.75 ± 0.087
3.9	1.24 ± 0.074
4.2	0.7 ± 0.06
4.5	0.61 ± 0.06
4.8	0.58 ± 0.058

height shown in Figs. 3 and 4 is above all the theoretical predictions presented there, it seems unlikely that the actual value of the cross-section maximum is even larger than displayed. Multiplication by a scale factor of less than 1.0 would improve the agreement regarding the height of the peak, but at the same time deteriorate it on the edges of the energy regime for which the experiment was performed. We are not confident hypothesizing whether the resonance or the background is calculated more accurately, or whether the experimental data are significantly more accurate in one regime than in another. Nevertheless, we present absolute experimental data in Table III, but with the conservative estimate of a possible scale factor in the range 0.5–1.1.

We finish the presentation of our results with Fig. 5, which presents a comparison of the excitation functions for the $^2D_{5/2}$ and $^2D_{3/2}$ states, and the dominant partial-wave contributions, as obtained in the fully relativistic DBSR34 model. Similar to the case of e-Au collisions [7], there is a strong violation of the statistical branching ratio of 3:2 in favor of exciting the $^2D_{5/2}$ state, which would be obtained in a purely nonrelativistic model after recoupling the results and ignoring the energy splitting between the two fine-structure levels. We see that the principal reason for the deviation from the statistical branching ratio is the fact that the broad maxima are due to different angular-momentum symmetries of the e-Cu collision system, namely $J = 1^-$ for the $^2D_{3/2}$ state and $J = 2^-$ for the $^2D_{5/2}$ state, respectively. In a nonrelativistic picture, both symmetries contain contributions from an incident p wave, with the f wave also contributing to $J = 2^-$. Most interestingly, we see that only odd-parity symmetries, corresponding to incident and outgoing p and f waves, contribute significantly to the cross section. This suggests that the direct quadrupole-type $3d \rightarrow 4s$ one-electron transition process is much less important than the dipole-driven exchange process, in which an incident p or f continuum electron interacts with the active target electron

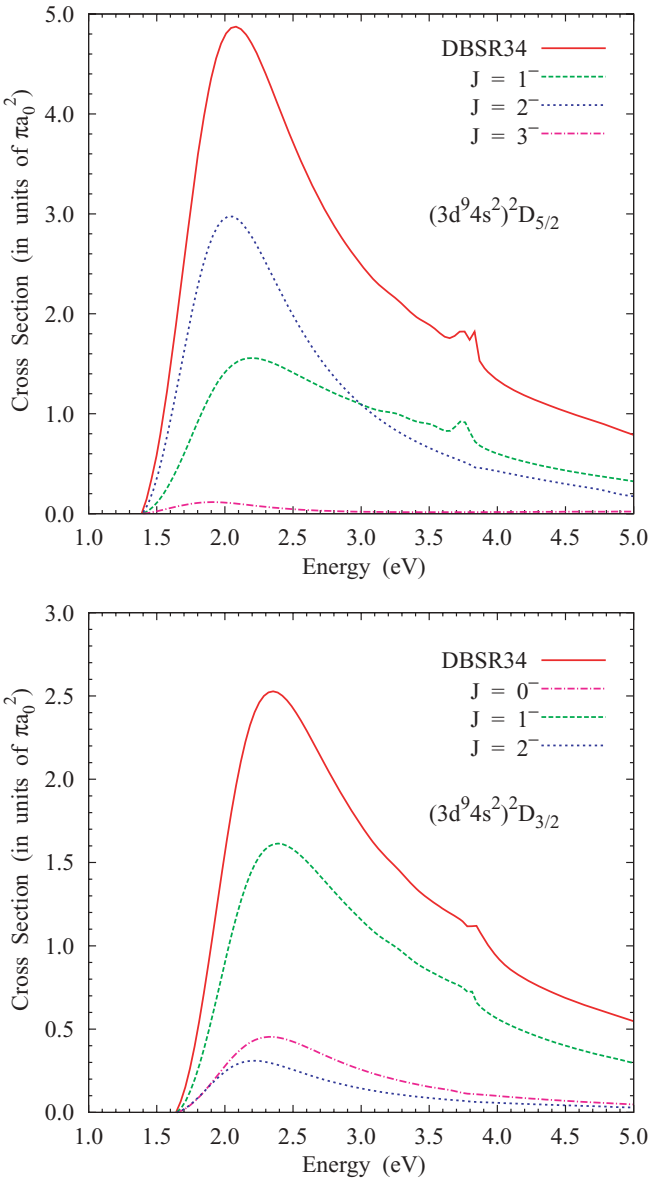

FIG. 5. (Color online) Dominant partial-wave contributions to the excitation functions of the $^2D_{5/2}$ and $^2D_{3/2}$ states, as obtained in the DBSR34 model. The solid lines represent the sums of the contributions, while the individual partial-wave contributions are labeled in the legend.

in a complicated manner, ultimately leading again to a free electron with $l = 1$ or $l = 3$.

V. SUMMARY AND CONCLUSIONS

We have presented results from a joint experimental and theoretical study of electron impact excitation of the $(3d^{10}4s)^2S_{1/2} \rightarrow (3d^9 4s^2)^2 D_{5/2,3/2}$ transitions in copper atoms. The experimental results were obtained with the laser-induced fluorescence technique, and the validity of the Percival-Seaton hypothesis regarding the vanishing role of the nuclear spin was explicitly verified. The calculations were performed using nonrelativistic, semirelativistic, and fully relativistic R-matrix (close-coupling) approaches, including a recently developed fully relativistic and general B-spline

R-matrix code that allows for the treatment of complex atomic and ionic targets. In particular, relaxation effects in the one-electron orbitals and core-valence correlation can be treated ab initio and consistently in both the structure and the collision calculations. While the predictions from the various theoretical models appear to be internally consistent, in agreement with general expectations regarding the importance of relativistic effects for a target such as copper, a significant difference in the observed and the calculated position of the near-threshold maximum in the excitation function of the $(3d^9 4s^2)^2 D_{3/2}$ state remained. Having currently no explanation for this remaining discrepancy, we hope that the work reported here will stimulate future efforts, both experimentally and theoretically, on this very challenging collision problem.

ACKNOWLEDGMENTS

The calculations were performed at the Texas Austin Computer Center (Ranger) through a Teragrid allocation. This work was supported by the US National Science Foundation (O.Z. and K.B.) and by the Australian Research Council (V.S., M.J.B., and P.J.O.T.). K.B. wishes to thank Flinders University for travel assistance during his visit.

[1] A. Kearsley, in *SPIE Proceedings, Bellingham, 1990* (SPIE, Bellingham, 1990), Vol. 1225, p. 271.
[2] V. Suvorov, P. J. O. Teubner, V. Karaganov, K. Ratnavelu, Y. Zhou, and M. J. Brunger, Phys. Rev. A **80**, 022711 (2009).
[3] G. G. Petrash, Usp. Fiz. Nauk **14**, 747 (1972).
[4] K. F. Scheibner, A. U. Hazi, and R. J. W. Henry, Phys. Rev. A **35**, 4869 (1987).
[5] K. F. Scheibner and A. U. Hazi (private communication).
[6] M. Maslov, M. J. Brunger, P. J. O. Teubner, O. Zatsarinny, K. Bartschat, D. V. Fursa, I. Bray, and R. P. McEachran, Phys. Rev. A **77**, 062711 (2008).
[7] O. Zatsarinny, K. Bartschat, M. Maslov, M. J. Brunger, and P. J. O. Teubner, Phys. Rev. A **78**, 042713 (2008).
[8] O. Zatsarinny and C. Froese Fischer, J. Phys. B **33**, 313 (2000).
[9] O. Zatsarinny and K. Bartschat, J. Phys. B **37**, 2173 (2004).
[10] O. Zatsarinny and K. Bartschat, Phys. Rev. A **77**, 062701 (2008).
[11] O. Zatsarinny, Comput. Phys. Commun. **174**, 273 (2006).
[12] W. R. MacGillivray and M. C. Standage, Phys. Rep. **168**, 1 (1988).
[13] P. G. Pappas, M. M. Burns, D. D. Hinshelwood, and M. S. Feld, Phys. Rev. A **21**, 1955 (1980).
[14] V. Suvorov, Ph.D. thesis, Flinders University of South Australia, 1996.
[15] I. C. Percival and M. J. Seaton, Proc. Camb. Phil. Soc. **53**, 654 (1958).
[16] M. J. Brunger and W. Adcock, J. Chem. Soc. Perkin Trans. **2**, 1 (2002).
[17] S. J. Buckman, P. Hammond, G. C. King, and F. H. Read, J. Phys. B **16**, 4219 (1983).
[18] K. A. Berrington, W. N. Eissner, and P. N. Norrington, Comput. Phys. Commun. **92**, 290 (1995).
[19] E. Clementi and C. Roetti, At. Data Nucl. Data Tables **14**, 177 (1974).
[20] A. Hibbert, Comput. Phys. Commun. **9**, 141 (1975).
[21] C. Froese Fischer, T. Brage, and P. Jönsson, *Computational Atomic Structure: An MCHF Approach* (Institute of Physics Publishing, Bristol, 1997).
[22] O. Zatsarinny and C. Froese Fischer, J. Phys. B **35**, 4669 (2002).
[23] P. Jönsson, X. He, C. Froese Fischer, and I. P. Grant, Comput. Phys. Commun. **177**, 597 (2007).
[24] C. Froese Fischer, J. Phys. B **10**, 1241 (1977).
[25] V. M. Burke and C. J. Noble, Comput. Phys. Commun. **85**, 471 (1995).
[26] C. E. Moore, *Atomic Energy Levels*, Vol. 3, NSRDS-NBS 35 (US Government Printing Office, Washington, DC, 1971) [http://physics.nist.gov/cgi-bin/AtData/levels_form].
[27] J. E. Sansonetti and W. C. Martin, J. Phys. Chem. Ref. Data **34**, 1559 (2005).
[28] C. Froese Fischer and O. Zatsarinny, Comput. Phys. Commun. **180**, 879 (2009).
[29] [http://www.netlib.org/scalapack].